Weakly nonlinear analysis of the flutter motion of thin cylinders

Joël Tchoufag, David Fabre, Jacques Magnaudet

Weakly Nonlinear Analysis Of The Flutter Motion of Thin Cylinders.

Joël TCHOUFAG[1], David FABRE[1], Jacques MAGNAUDET[2]

[1] *Université de Toulouse, Institut de Mécanique des Fluides de Toulouse, Av. du Prof. Camille Soula, 31400 Toulouse, France*
[2] *CNRS, IMFT,F-31400 Toulouse*

Abstract.

The nature overflows of examples which prove that buoyancy-driven objects in a viscous medium can result in diverse and exotic trajectories. Among them is found the so-called Zig-Zag (ZZ) path or flutter which we investigate in the present work. The configuration is that of a thin cylinder initially rising/falling vertically in an unbounded fluid otherwise at rest. The problem is parametrized by the aspect ratio (diameter to thickness) χ, the moment of inertia I^* and Archimedes number (gravitational-velocity-based Reynolds) Ar. For small I^*, past studies have reported a supercritical transition from the vertical to the ZZ path at a critical Ar_c. We show by means of linear and weakly nonlinear analyses that the observed flutter results from the nonlinear saturation of an unstable global mode of the coupled fluid+disk problem.

Key words: wake, instability, asymptotic expansion.

1 Introduction

The problem of a freely falling or rising body in a viscous fluid is quite fascinating. Even simple objects such as coins falling in a newtonian fluid have been known for centuries as able to undergo chaotic trajectories as well as regular ones such as flutter or tumbling. From falling leaves and seeds in ecology to the freefall of a spacecraft through rarified atmosphere in aeronautics, the wide range of applications of this problem has led, particularly in the last decade, to several experimental, numerical and theoretical works (see Ern *et al.* 2012, for a comprehensive review). Tackling this complex problem from a stability point of view, we recently carried out the linear stability analysis of the coupled fluid-body problem in the case of two-dimensional objects such as thin plates and rectangular rods [1] and axisymmetric bodies, namely disks of finite thickness[14]. Now, the aim of this study is to predict the characteristics of the flutter motion (ZZ) systematically undergone by thin cylinders initially rising or falling in a steady vertical (SV) manner. The paper is organized as follows. After describing the relevant parameters and the governing equations of the problem, we will briefly give some results of the linear stability analysis of the coupled fluid+disk system. We shall then proceed with the analysis of a third order weakly nonlinear expansion of this system. To assess the validity

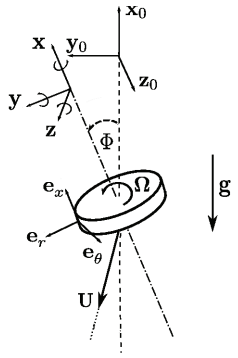

Figure 1: Problem configuration. The disc is assumed to be initially released with its axis oriented in the vertical direction. Gravity oriented downwards, discs such that $\bar{\rho} > 1$ fall whereas light discs with $\bar{\rho} < 1$ rise.

of our asymptotic model, we will compare the amplitude and the frequency of our asymptotic model to existing experimental and DNS data.

2 Problem formulation

We consider a thin cylinder (hereinafter referred to as 'disc') of thickness h, diameter d and density ρ_b falling or rising freely under gravity in an unbounded fluid of kinematic viscosity ν and density ρ, at rest at infinity. The disc is of volume $\mathscr{V}$, mass M and moment of inertia tensor $\mathbb{I}$. Let $\mathbf{U}(t)$ and $\mathbf{\Omega}(t)$ be the translational and rotational components of the instantaneous velocity of the moving object as shown on figure 1. The problem is then entirely defined by three dimensionless parameters: the Reynolds number $Re_b = \|\mathbf{U}\|d/\nu$, the aspect ratio $\chi = d/h$ and the body-to-fluid density ratio $\bar{\rho} = \rho_b/\rho$ sometimes replaced by the dimensionless inertia $I^* = \frac{\pi}{64}\bar{\rho}/\chi$ (which reads $\frac{\pi}{64}\sigma_b/\rho d$ when $\chi \to \infty$ with σ_b the surface density). Since the disc velocity is usually not known beforehand, Re_b is strictly speaking not a control parameter of the problem and is advantageously replaced by the so-called Archimedes number $Ar = \sqrt{\frac{3}{32}}U_g d/\nu$ based on the gravitational velocity $U_g = (2|\bar{\rho} - 1|gh)^{1/2}$.

At least two frames of reference, sketched in figure 1, will be of interest here: the absolute or laboratory frame $(O, \mathbf{x_0}, \mathbf{y_0}, \mathbf{z_0})$ and the relative or body frame $(C, \mathbf{x}, \mathbf{y}, \mathbf{z})$ where C in the disc's center of mass. In the first one, we define the distance vector $\mathbf{CM} = \mathbf{r}$ for any material point M, and the vector $\mathbf{\Phi} = (\zeta, \Xi, \Psi)$ characterizing the roll/pitch/yaw of the system. That is, rotations about $\mathbf{x}, \mathbf{y}$ and $\mathbf{z}$, respectively. Last, the rotation rate is defined as $\mathbf{\Omega} = d\mathbf{\Phi}/dt$. The elasticity of the considered body being neglected (no possible buckling and flapping), the trajectory of the disk is described by the rigid-body motion equations and the flow around it by the Navier-Stokes equations. The system of equations governing the fluid+disc dynamics is fully coupled through the fluid forces and torques acting on the disc's surface $\mathscr{S}$ on the one hand and the no-slip boundary condition on $\mathscr{S}$ imposed to the flow by the moving disc on the other hand. Written in the absolute reference frame but with axes rotating with the disc [10], the full set of equations reads:

$$\nabla \cdot \mathbf{V} = 0 \quad , \tag{1}$$

$$\frac{\partial \mathbf{V}}{\partial t} + (\mathbf{V} - \mathbf{W}) \cdot \nabla \mathbf{V} + \mathbf{\Omega} \times \mathbf{V} = -\frac{1}{\rho} \nabla P + \nu \nabla^{\mathbf{2}} \mathbf{V} \quad , \tag{2}$$

$$M \frac{\mathrm{d}\mathbf{U}}{\mathrm{d}t} + M \mathbf{\Omega} \times \mathbf{U} = (M - \rho \mathscr{V}) \mathbf{g} + \int_{\mathscr{S}} \mathbf{T} \cdot \mathbf{n} \mathrm{dS} \quad , \tag{3}$$

$$\mathbb{I} \cdot \frac{\mathrm{d}\mathbf{\Omega}}{\mathrm{d}t} + \mathbf{\Omega} \times (\mathbb{I} \cdot \mathbf{\Omega}) = \int_{\mathscr{S}} \mathbf{r} \times (\mathbf{T} \cdot \mathbf{n}) \mathrm{dS} \quad , \tag{4}$$

$$\frac{\mathrm{d}\mathbf{\Phi}}{\mathrm{d}t} = \mathbf{\Omega} \quad , \tag{5}$$

where $\mathbf{V}(\mathbf{r}, t)$ and $P(\mathbf{r}, t)$ are the velocity and pressure fields in the fluid, $\mathbf{W}(\mathbf{r}, t) = \mathbf{U}(t) + \mathbf{\Omega}(t) \times \mathbf{r}$ is the local entrainment velocity, $\mathbf{T} = -P\mathbf{I} + \rho\nu(\nabla \mathbf{V} + {}^{\mathbf{t}}\nabla \mathbf{V})$ denotes the stress tensor and $\mathbf{I}$ is the Kronecker tensor. Finally, the no-slip condition on the disc surface and the vanishing of the fluid velocity at large distance imply $\mathbf{V} = \mathbf{W}$ on $\mathscr{S}$ and $\mathbf{V} = \mathbf{0}$ for $\|\mathbf{r}\| \to \infty$.
The problem is solved numerically, using the finite elements software FreeFem++ (http://www.freefem++.org). The equations governing the disc motion are projected onto $(\mathbf{x}, \mathbf{y}, \mathbf{z})$ and those governing the fluid onto the local cylindrical basis $(\mathbf{e}_r, \mathbf{e}_\theta, \mathbf{x})$ (see figure 1). The computational domain is made of triangular elements and local refinements are applied to capture properly the boundary layer and near wake of the disc.

3 Weakly Nonlinear Stability Analysis

To perform the weakly nonlinear stability analysis (WNA) of the problem, we proceed in the line of past studies dealing with instabilities in the wake of a fixed bluff body[13, 9]. The procedure relies on a multiple time scale technique involving a fast and a slow time scale, namely t and $\tau = \epsilon^2 t$. Note that this formalism is different from the weakly nonlinear analysis recently performed on the oblique motion of discs and spheres[6]. We assume the following asymptotic expansion:

$$\epsilon^2 = \frac{\delta}{Ar_c^2} \tag{6a}$$

$$\mathcal{Q} = \mathcal{Q}_{\mathbf{0}} + \epsilon \mathbf{q_1}(\mathbf{t}, \tau) + \epsilon^{\mathbf{2}} \mathbf{q_2}(\mathbf{t}, \tau) + \epsilon^{\mathbf{3}} \mathbf{q_3}(\mathbf{t}, \tau) + \cdots . \tag{6b}$$

With $\epsilon \ll 1$ and $\delta = Ar - Ar_c$ the departure from criticality where the steady flow $\mathbf{Q_0}$ is linearly unstable. The state vector is made of the set of variables associated to the fluid and the disc and reads $\mathcal{Q} = [\mathbf{V}(\mathbf{r}, t), P(\mathbf{r}, t), \mathbf{U}(t), \mathbf{\Omega}(t), \mathbf{\Phi}(t)]$ in the most general case. Introducing the above ansatz into (5), a zeroth-order non-linear problem, higher-order linear problems are obtained, all of which are rewritten in a weak formulation and then projected onto the finite elements basis. The latter is made of P2 (quadratic) elements for the velocity field and P1(linear) for the pressure. The obtained matrices are inverted by the LU solver of the embedded UMFPACK library, while the SLEPc library is employed to compute the generalized eigenpairs of the first order linear stability problem.

3.1 Zeroth order: base flow

The zeroth-order flow, also known as the base flow, is sought in the form of a steady axisymmetric flow associated with a steady vertical broadside motion of the disc. Therefore, the corresponding state vector $\mathcal{Q}_\mathbf{0} = [\mathbf{V_0}(\mathbf{r}), P_0(\mathbf{r}), -U_0\mathbf{x}, \mathbf{0}, \mathbf{0}]$. From now on, the governing equations and problem variables will be made dimensionless. Interestingly, when equation (3), which reduces to a balance between the net weight of the disc and the drag force, is adimensionalized, it comes:

$$Ar^2 = \frac{3}{32} Re^2 C_D(Re) \quad , \tag{7}$$

where $C_D = 8D_0/\pi$ denotes the dimensionless drag coefficient and now $Re = U_0 d/\nu$. In what follows, the stability analysis is carried out for fixed values of Re, i.e. for imposed values of the settling/rise velocity. Nevertheless, for the sake of comparison with experimental and computational studies in which the actual control parameter is the Archimedes number, the corresponding values of Ar will be systematically computed using (7). This correspondence is exact as long as the threshold at which the steady vertical motion of the body is destabilized is concerned. After this primary bifurcation at Re_c, we perform a first order Taylor expansion of (7) around Re_c to obtain the modified $Ar = f(Re)$ relationship. Using an iterative Newton method, the base flow is obtained by solving the incompressible steady Navier-Stokes equations supplemented with the no-slip condition ($\mathbf{V_0} = -\mathbf{x}$) on the disc and the far-field condition $\mathbf{V_0} = \mathbf{0}$. Figure 2 shows an example of the base flow in the case of an extremely thin disc at a Reynolds number $Re = 94$. As one could expect, the wake structure is exactly that of the axisymmetric flow past a fixed disc, viewed in the laboratory frame. The drag coefficient $C_D \simeq 1.20$ compares well with the value $C_D \simeq 1.23$ determined experimentally by [12].

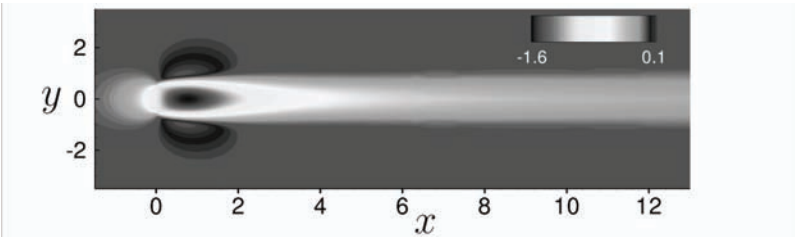

Figure 2: Typical base flow: case of an extremely thin disc ($\chi = 10^4$) falling at $Re = 117$. The colour scale refers to the magnitude of the axial velocity. The gravity vector is oriented to towards the left.

3.2 First order: linear stability analysis

At order ϵ, the linearized form of Eq. (5) are obtained and recast in a matrix form as $\partial_t \mathscr{B}\mathbf{q_1} + \mathscr{A}\mathbf{q_1} = \mathbf{0}$. The long-term solution of this problem can be sought as the superposition of its linearly unstable modes, the stable ones eventually vanishing. In particular, we search for normal modes, i.e :

$$\mathbf{q_1} = \begin{pmatrix} \hat{\mathbf{q}}^f_{1m}(r,x)e^{\mathrm{i}m\theta} \\ \hat{\mathbf{q}}^b_{1m}(x,y,z) \end{pmatrix} e^{\lambda t} + c.c. \quad , \tag{8}$$

Where *c.c.* denotes the complex conjugate and $\hat{\mathbf{q}}_{1m} = (\hat{\mathbf{q}}_1^f, \hat{\mathbf{q}}_{1m}^b)^T$ is the global mode of azimuthal wavenumber m associated to the complex eigenvalue $\lambda = \lambda_r + \mathrm{i}\lambda_i$ whose real and imaginary parts are the growth rate and frequency of the mode, respectively. Note the relevant unknowns in $\hat{\mathbf{q}}_{1m}$ and the boundary conditions on the disk and for the far-field depend on m [14]. The first order linear problem thus gives, for each m, a generalized eigenproblem $\lambda\mathscr{B}_m\hat{\mathbf{q}}_{1m} + \mathscr{A}_m\hat{\mathbf{q}}_{1m} = \mathbf{0}$. Rather than solving for every m, computations are limited in practice to the subspace $m > 0$ due some spatial symmetry[9]. Given an axisymmetric disc of aspect ratio χ, one can compute the eigenpairs $(\lambda, \hat{\mathbf{q}})$ for various sets of Ar and I^*. We find that $|m| = 1$ modes are the most amplified ones, as in the case of wake instability past fixed 3D bluff bodies [11]. Moreover, it can be shown that modes such that $|m| \geq 2$ only act on the fluid, as if the disc were held fixed regardless of its mass[14]. Therefore, they are not involved in the fluid-body coupling and this WNA shall show that they are not required to capture the oscillations of the bodies. For the sake of conciseness, we shall only display on figure 3 the structure of the unstable global mode underneath the primary destabilization of the SV rise of a $\chi = 3$ disc with $\bar{\rho} = 0.99$. In the following, only this value of $\bar{\rho}$ shall be used for comparison with experiments and DNS.

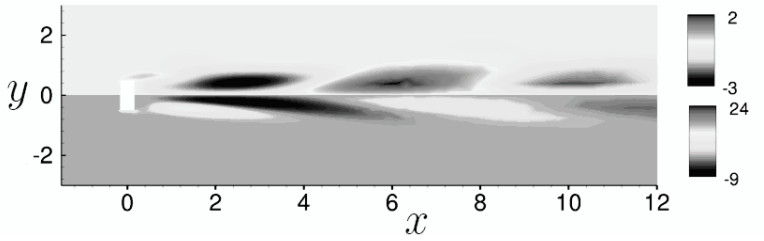

Figure 3: Structure the global mode a disc $\chi = 3$ at its threshold. The axial velocity (resp. axial vorticity) is shown on the upper (resp. lower) part and normalized with respect to the inclination.

The alternate positive/negative disturbances shows the oscillating character of the mode. This instability corresponds to an Hopf bifurcation at $Ar_c \simeq 44.98$ and matches with the transition to flutter observed in DNS[2] at $Ar_c^{DNS} \simeq 44.8$ and experiments[7] at $Ar_c^{EXP} \simeq 46$. Since it is normalized so that $\|\boldsymbol{\phi}\| = 1$, the same order of magnitude for the levels of axial velocity denote a strong coupling between the disc and the surrounding fluid. Bearing in minde that only the fluid variables depend on the azimuthal direction, we write the first order solution as:

$$\mathbf{q_1} = A^+(\tau)\hat{\mathbf{q}}_{A^+}e^{\mathrm{i}\theta+\mathrm{i}\lambda_i t} + A^-(\tau)\hat{\mathbf{q}}_{A^-}e^{-\mathrm{i}\theta+\mathrm{i}\lambda_i t} + c.c. \tag{9}$$

When $Ar > Ar_c$, it is the amplitudes $A^\pm$ that grows exponentially in this ϵ-order approximation, before saturating as we show below.

3.3 Higher orders: Landau amplitude equation

At order ϵ^2, the governing equations can be written as

$$\partial_t\mathscr{B}\mathbf{q_2} + \mathscr{A}\mathbf{q_2} = \mathbf{F_2}(\mathbf{Q_0}, \mathbf{q_1}). \tag{10}$$

The forcing on the right hand side is made of seven independant terms from three sources: the effect of a small variation of Ar, the interactions of $(\mathbf{q_{A^\pm}} + c.c.)$ with

itself and at last the interactions between ($\mathbf{q_{A^+}} + c.c.$) and ($\mathbf{q_{A^-}} + c.c.$). Solving the linear system (10) for each contribution of the forcing results in a solution of the form [9]:

$$\begin{aligned}\mathbf{q_2} &= \hat{\mathbf{q}}_\delta + |A^+|^2\hat{\mathbf{q}}_{A^+A^{+*}} + |A^-|^2\hat{\mathbf{q}}_{A^-A^{-*}} \\ &\quad + A^+A^{-*}\hat{\mathbf{q}}_{A^+A^{-*}}e^{2\mathrm{i}\theta} + A^+A^-\hat{\mathbf{q}}_{A^+A^-}e^{2\mathrm{i}\lambda_i t} + c.c. \\ &\quad + A^{+2}\hat{\mathbf{q}}_{A^+A^+}e^{2\mathrm{i}\theta+2\mathrm{i}\lambda_i t} + A^{-2}\hat{\mathbf{q}}_{A^-A^-}e^{-2\mathrm{i}\theta+2\mathrm{i}\lambda_i t} + c.c. \end{aligned} \tag{11}$$

The problem at order ϵ^3 is once again an inhomogeneous linear system with a forcing $\mathbf{F_3}(\mathbf{Q_0}, \mathbf{q_1}, \mathbf{q_2})$. However, $\mathbf{F_3}$ contains terms which go as $\sim e^{\pm\mathrm{i}\theta\pm\mathrm{i}\lambda_i t}$. Such terms are known as resonant forcing because they are exciting the unstable global modes of the fluid+disc system which could then experience resonance. In order to avoid these secular responses and solve the expansion at the third order, we use the Fredholm alternative and impose compatibility conditions. That is, the resonant forcing terms must be orthogonal to the kernel (modes) of the adjoint operator of the linearized operator ($\partial_t\mathscr{B}+\mathscr{A}$). This condition leads to the following system of complex amplitude equations (or normal form):

$$\frac{dA^\pm}{d\tau} = \frac{1}{\epsilon^2}\frac{dA^\pm}{dt} = \sigma A^\pm - \mu A^\pm|A^\pm|^2 - \nu A^\pm|A^\mp|^2. \tag{12}$$

Where σ is the exponential growth rate in the linear regime, while μ and ν are coefficients which depend on the normalization of the global modes and express the intensity of the interactions causing the nonlinear saturation. This is the classical normal form for a Hopf bifurcation. It has two non trivial solutions: the rotating wave (RW) involving only one spiral mode and the standing wave (SW) corresponding the superimposition of both counter-rotating modes $\mathbf{q_{A^+}}$ and $\mathbf{q_{A^-}}$. RW is super(sub)-critical if $\mu_r > 0 (< 0)$ and stable (i.e observed in experiments) if $\mu_r < \nu_r$. SW is super(sub)-critical if $(\mu_r + \nu_r) > 0 (< 0)$ and is the observed solution when $\nu_r < \mu_r$. The magnitude and the frequency (Strouhal number) of the limit cycles of these solutions read:

$$|A^\pm|_{SW} = \epsilon\sqrt{\frac{\sigma_r}{\mu_r+\nu_r}} \qquad St_{SW} = St_0 + \epsilon^2\sigma_i - |A|_{SW}(\mu_i+\nu_i) \tag{13}$$

$$|A^\pm|_{RW} = \epsilon\sqrt{\frac{\sigma_r}{\mu_r}} \qquad St_{RW} = St_0 + \epsilon^2\sigma_i - |A|_{RW}(\mu_i) \tag{14}$$

Where $St_0 = \lambda_i d/(2\pi U_0)$. In terms of trajectory, while RW and SW respectively correspond to an helical and a Zig-Zag path. The coefficients of (12) have been computed for discs of different thickness, A denoting the inclination of the disc.

3.3.1 Case 1: $\chi = 3$, $\bar{\rho} = 0.99$

The vertical rise is linearly unstable at $Ar_{c1} = 44.98$ via a Hopf bifurcation and we obtain $\sigma_1 = 69.62 + \mathrm{i}39.873$, $\mu_1 = 11.02 + \mathrm{i}0.084$ and $\nu_1 = 6.11 + \mathrm{i}7.703$. Therefore, according to the aforementioned criteria the branch SW will be selected at Ar_{c1} in agreement with DNS and experimental data where the flutter motion is observed for $Ar \gtrsim 45$. More quantitatively, figure 4(a) shows that the prediction given by Eq. (13) correctly matches the amplitude of the disc inclination in the ZZ regime. Regarding the frequency of the flutter, we empirically find that experimental and

numerical data are best approached by $\tilde{St}_{RW}$ which is a modified expression of St_{RW} obtained by replacing in that of Eq. (14) the amplitude $|A|_{RW}$ by $|A|_{SW}$. Figure 4(a) shows that the amplitude of oscillations predicted by the WNA is still accurate for Ar where the assumption $\epsilon \ll 1$ fails, contrary to the frequency shown on figure 4(b) which renders a more expected picture.

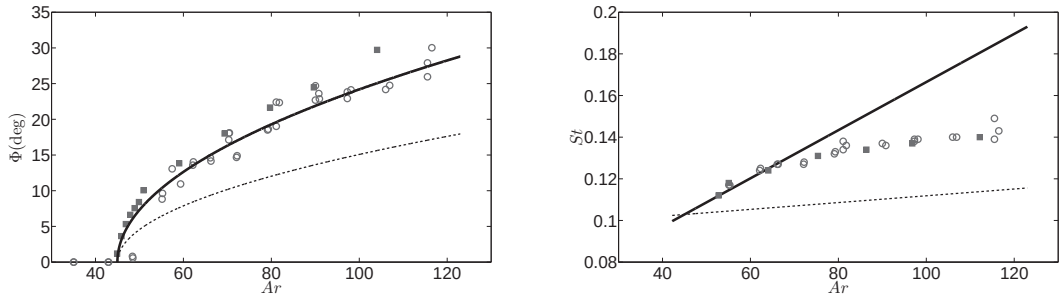

(a) (b)

Figure 4: Case of a thin cylinder $\chi = 3$. The open circles are from experiments[8] and the filled squares from DNS [2]. (a) Inclination: the solid (dashed) line corresponds to $\Phi = 2|A|_{SW}$ ($\Phi = |A|_{RW}$). (b) Frequency of the limit cycle: the solid line corresponds to $\tilde{St}_{RW}$ (see text) while the dashed line is St_{SW}.

3.3.2 Case 1: $\chi = 6$, $\bar{\rho} = 0.99$

The primary instability occurs at $Ar_{c2} = 41.78$ through a Hopf bifurcation and the coefficients of the normal form are $\sigma_2 = 70.07 + \mathrm{i}26.97$, $\mu_2 = 11.57 - \mathrm{i}8.603$ and $\nu_2 = 14.54 + \mathrm{i}7.17$. This implies that the RW is the stable branch in agreement with experimental observation by Fernandes *et al.* who reported that for the disc $\chi = 6$, there is a transition at $Ar \approx 43$ to an helical regime which then leads to the flutter motion at higher Ar[8]. Note that in practice, neither is the ZZ perfectly planar nor the helical path an exact circular helix. Therefore, one segregates between these regimes by defining the ratio $\eta = \tilde{z}/\tilde{y}$ of the amplitudes of the horizontal body displacements such that $\eta = 0$ (resp. $\eta = 1$) for the plane ZZ (resp. circular helix). The red line in figure 5(a) shows the experimental limit $\eta_l \simeq 0.7$ at $Ar_l \simeq 54$ between a rather spiral path close to Ar_{c2} and a rather planar ZZ far from it. The WNA proves again here to be valid since the branch $|A|_{RW}$ and St_{RW} capture well the experimental and numerical amplitude and the frequency of the oscillations in the vicinity of the threshold. Last, note that despite being unstable, the SW branch provides rather good prediction for the ZZ regime undergone by the disc for $Ar > Ar_l$. However, we find that in this range, St_{RW} fits unexpectedly better than St_{SW} the reported frequency up to $Ar \approx 70$. These results are still unexplained at this stage of our investigations.

3.3.3 Towards a unique law for the flutter of finite thickness discs

For thin cylinders of aspect ratio $\chi > 8$ initially in the SV regime, the flutter motion is observed after at least intermediate two bifurcations[2, 4]. However, though the

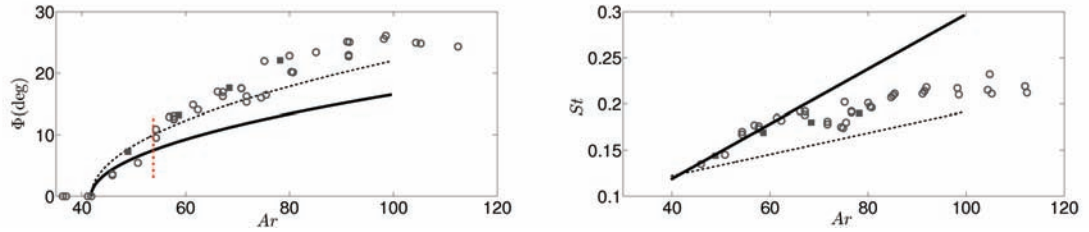

(a) (b)

Figure 5: Case of a thin cylinder $\chi = 6$. The open circles are from experiments[8] and the filled squares from DNS [4]. (a) Inclination: the solid (dashed) line corresponds to $\Phi = |A|_{RW}$ ($\Phi = 2|A|_{SW}$). The red dos-dashed line separates the spiral and flutter regimes. (b) Frequency of the limit cycle: the solid (dashed) line corresponds to St_{RW} (St_{SW}).

transition sequence is different, Fernandes *et al.* evidenced for $\chi \in [2, 10]$ that once the ZZ is reached, it could be characterized by one single empirical law for its amplitude and another one for the frequency (see figures 18-20 in [8]). For this matter, some quantities must be rescaled. Specifically, St is replaced by $St^* = St(2/C_D)^{1/2}\chi^{-1/2}$ and Ar by the control parameter $Re^* = V_w d/\nu$ where V_w is the maximum velocity of the recirculation bubble in the lee of the disc. Re^* has the advantage of yielding a χ-independant threshold for the transition SV-to-ZZ, due to the fact that $Re^* = 0.62(1 + \chi^{-1}Re_m)$ where Re_m is the Reynolds number based on the time-average settling/rise body velocity[8]. Moreover, since $Ar \approx 0.34Re_m$ for the whole range of $\chi \leq 10$ as shown in[8], we are able to relate Ar to Re^* and compare our WNA prediction to experimental data. Figure 6(a) and (b) respectively show the $|A|_{SW}$ and $\tilde{St}_{RW}$ branches for $\chi = 2$ and $\chi = 3$.

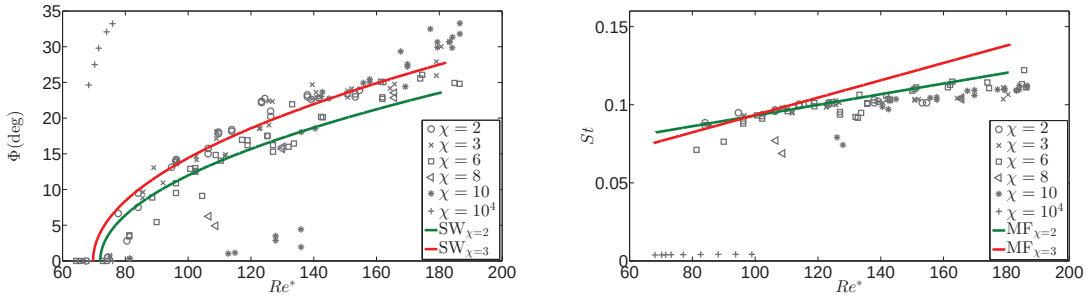

(a) (b)

Figure 6: (a)Inclination $|\Phi|_{SW}$ and (b)Strouhal $\tilde{St}^*_{RW}$ as function of Re^*. The symbols for $\chi \leq 10$ are from experiments[8] and those at $\chi = 10^4$ from DNS[2]. The red (green) line is the WNA model for $\chi = 3$ ($\chi 2$)

The WNA applied to both discs provide a good estimation of the amplitude and the frequency of oscillations in the flutter regime for $\chi \leq 10$. The fact that the branches do not superimpose may imply that even the choice of Re^* as the control parameter does not allow to completely get rid of the aspect ratio. This idea is supported by

the non-negligeable scatter of the experimental data.
The flutter motion of thin cylinders at moderate Reynolds number is thus a supercritical Hopf bifurcation which obeys a unique law $\Phi = P_1(Re^* - Re_c^*)^{1/2}$ for its inclination and $St^* = 0.103 + S_1(Re^* - Re_c^*)$ where P_1,S_1 and S_2 are constant. We obtain $S_1 = 3.86\&P_1 = 0.049$ for $\chi = 2$ and $S_1 = 4.89\&P_1 = 0.061$ for $\chi = 3$ in agreement with $P^{EXP} = 0.058$ obtained by a best-fit of experimental data[8]. However, this behavior fails for $\chi \to \infty$ as illustrated here for an extremelety thin disk $\chi = 10^4$. This failure has a two-fold explanation. On one hand, the ZZ of an infinitely thin disc has a subcritical nature [2, 4] for $\bar{\rho} = 0.99$ and can thus exhibit large amplitudes before the linear stability threshold as seen on figure 6 (a). On the other hand, the expression $St^* \sim (C_D\chi)^{-1/2}$ goes to zero when $\chi \to \infty$ given that $C_D \sim O(1)$. Therefore, it is inconsistent with the flutter of a disc which is a high-frequency unsteady motion. This suggests the existence of a cut-off aspect ratio between 10 and 10^4 below which the transition to ZZ is supercritical and the frequency obeys $St^* \approx 0.1$.

4 Conclusions

We dealt in this study with the stability of a buoyancy-driven thin cylinder of aspect ratio χ, initially in a steady vertical motion. We carried out a weakly nonlinear analysis (WNA) of this configuration derived for control parameters in the vicinity of criticality, where the coupled fluid+disc system is linearly unstable. It was found that for $\chi < 8$, the SV regime becomes unstable at an almost constant threhold Ar_c and bifurcates via a Hopf bifurcation to the ZZ regime except for $\chi = 6$ where an helical motion is undergone in a small range of $Ar > Ar_c$ before leading eventually leading to the ZZ. Although the route to the flutter is more complex for thinner cylinders, it was shown that a unique law $A \sim (Re^* - Re^*)$ and $St^* \sim 0.1$ which is the signature of supercritical Hopf bifurcation characterizes well the ZZ oscillations of bodies with $\chi \leq 10$, Re^* being a Reynolds built on the recirculation-eddy maximum velocity. Systematic comparisons with experiments and DNS have proved that the amplitude and the frequency (Strouhal) of the flutter motion are accurately predicted by a third order weakly nonlinear expansion which leads to a complex Landau equation. The failure of the approach for extremely thin discs suggests the existence of a cut-off value χ_f between 10 and 10^4 beyond which the unique laws are no more valid. We aim in future investigations to determine χ_f with more precision. All the results presented here were obtained for $\bar{\rho} = 0.99$. Therefore, a next step will be to modify the inertia of the disc. More precisely, since codimension-two bifurcation points were observed for higher masses[14], we plan to tackle the steady/Hopf and Hopf/Hopf mode interactions in the vicinity of that kind of points. This would generalize such similar work recently performed on the wake of fixed discs and spheres[3, 5].

Acknowledgements

We warmly thank P. Fernandes, P. Ern and F. Risso for kingly giving us their experimental data, as well as F. Auguste for his constant help with the code JADIM

References

[1] P. Assemat, D. Fabre, and J. Magnaudet. The onset of unsteadiness of two-dimensional bodies falling or rising freely in a viscous fluid: a linear study. *J. Fluid Mech.*, 690:173–202, 2012.

[2] F. Auguste. *Instabilités de sillage générées derrière un corps solide cylindrique fixe ou mobile dans un fluide visqueux*. PhD thesis, Université de Toulouse, Toulouse, France, 2010.

[3] F. Auguste, D. Fabre, and J. Magnaudet. Bifurcation in the wake of a thick circular disk. *Theor. Comput. Fluid Dyn.*, 24:305–313, 2009.

[4] M. Chrust. *Etude numérique de la chute libre d'objets axisymétriques dans un fluide newtonien*. PhD thesis, Université de Strasbourg, Strasbourg, France, 2012.

[5] D. Fabre, F. Auguste, and J. Magnaudet. Bifurcation and symmetry breaking in the wake of axisymmetric bodies. *Phys. Fluids*, 20:051702, 2008.

[6] D. Fabre, J. Tchoufag, and J. Magnaudet. The steady oblique path of buoyancy-driven disks and spheres. *J. Fluids Mech.*, 707:24–36, 2012.

[7] P. C. Fernandes. *Etude expérimentale de la dynamique de coprs mobiles en ascension dans un fluide peu visqueux*. PhD thesis, Université de Toulouse, Toulouse, France, 2005.

[8] P. C. Fernandes, F. Risso, P. Ern, and J. Magnaudet. Oscillatory motion and wake instability of freely rising axisymmetric bodies. *J. Fluids Mech.*, 573:479–502, 2007.

[9] P. Meliga, J. M. Chomaz, and D. Sipp. Global mode interaction and pattern selection in the wake of a disk: a weakly nonlinear expansion. *J. Fluid Mech.*, 633:159–189, 2009.

[10] G. Mougin and J. Magnaudet. The generalized kirchhoff equations and their application to the interaction between a rigid body and a arbitrary time-dependent viscous flow. *Int. J. Mult. Flow*, 28:1837, 2002.

[11] R. Natarajan and A. Acrivos. The instability of the steady flow past spheres and disks. *J. Fluid Mech.*, 254:323–344, 1993.

[12] F. Roos and W. Willmarth. Some experimental results on sphere and disk drag. *AIAA Journal*, 9:285–291, 1971.

[13] D. Sipp and A. Lebedev. Global stability of base and mean-flows: a general approach and its applications to cylinder and open cavity flows. *J. Fluid Mech.*, 593:333–358, 2007.

[14] J. Tchoufag, D. Fabre, and J. Magnaudet. Global linear stability of the flow past buoyancy-driven thin cylinders and discs. *To be submitted*.